SIP (2013), vol. 2, e5, page 1 of 10 © The Authors, 2013.

doi:10.1017/ATSIP.2013.6

ORIGINAL ARTICLE

Reversible color transform for Bayer color filter array images

SUVIT POOMRITTIGUL[1], MASANORI OGAWA[1], MASAHIRO IWAHASHI[1] AND HITOSHI KIYA[2]

In this paper, we propose a reversible color transform (RCT) for color images acquired through a Bayer pattern color filter array. One existing RCT with fixed coefficients is simple to implement. However, it is not adaptive to each of input images. Another existing RCT based on eigenvector of covariance matrix of color components, which is equivalent to Karhunen–Loève transform (KLT), is adaptive. However, it requires heavy computational load. We remove a redundant part of this existing method, utilizing fixed statistical relation between two green components at different locations. Comparing to the KLT-based existing RCT, it was observed that the proposed RCT keeps adaptability and has better coding performance, even though its computational load is reduced.

Keywords: color, image, lossless

Received 1 July 2012; Revised 14 August 2013

I. INTRODUCTION

Data compression techniques have been widely used in storage and transmission of digital images. Most of those are based on lossy coding in which decoded images contain errors. Recently, lossless coding techniques have been utilized to preserve RAW images in its original form [1–4].

The Bayer pattern is one of the popular color filter arrays to acquire pixel values of the RAW image from a single image sensor [5]. So far, various types of lossless coding algorithms have been proposed for such images. Those are categorized into prediction based method [1–3, 6, 7] and transform-based method [4, 8–17].

A prediction-based method subtracts a weighted sum of neighboring pixel values from the current pixel value. Matsuda, *et al.* used neighboring pixels in the same component and also in different components to generate a prediction [1, 2]. It can utilize similarity between components (inter-color correlation), and also similarity between pixels inside a component (intra-color correlation).

Chung *et al.* proposed a simple procedure for prediction [3], and confirmed its superiority to the international standards JPEG LS [6], and JPEG 2000 [8]. They separated the original image into two sub-images. One contains all the green components G_0 and G_1, and the other contains red component R and blue component B. In this paper, we utilize their idea for simplification of our coding algorithm. However, the context modeling in the adaptive prediction in [3] requires heavy computational load. Therefore we construct a lossless coding based on a transform.

A transform-based method is composed of a reversible color transform (RCT) and a reversible wavelet transform. Zhang *et al.* decorrelated an input image with the Mallat's wavelet packet, and the output is encoded with the Rice code [4]. The JPEG 2000 also contains an RCT and a reversible wavelet based on the 5/3 tap filter bank [8], and the output is encoded with the EBCOT [18]. In [9], a simple RCT for the four components is reported (existing method I). It is quite simple to implement since its filter coefficients are fixed. However, those methods are not adaptive to correlation among color components of each input image due to their fixed coefficients.

To make it fully adaptive, an RCT can be constructed based on eigenvector of covariance matrix of color components. Its adaptability is essentially the same as the Karhunen–Loève Transform (KLT). So far, various RCTs based on KLT have been reported [10–15]. In [16, 17], permutations of Givens rotations implemented in the lifting structure were introduced to avoid the singular point problem (existing method II). However, it requires optimization of six rotation angles, and including them into compressed data as the overhead.

In this paper, we aim at constructing a "semi-adaptive" RCT for Bayer color filter array images with reduced computational load. We remove a redundant part of the lifting structure in the "full-adaptive" existing method II, utilizing a fact that statistical relation between the two green components G_0 and G_1 is almost fixed for various input

[1]Nagaoka University of Technology, Nagaoka, Niigata, 940-2188, Japan.
[2]Tokyo Metropolitan University, Hino, Tokyo, 191-0065, Japan.

Corresponding author:
Masahiro Iwahashi
Email: iwahashi@vos.nagaokaut.ac.jp

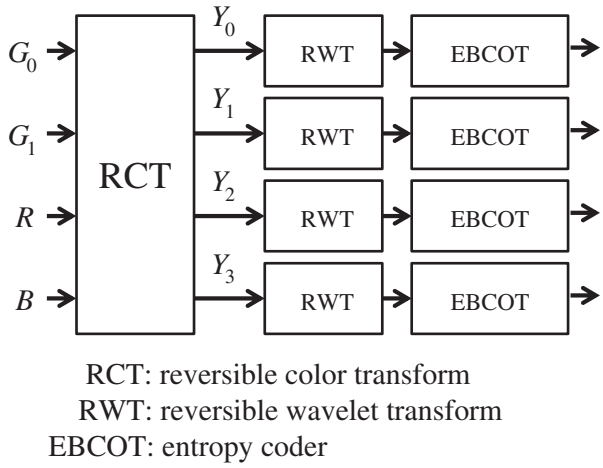

Fig. 1. Lossless coding system for Bayer pattern images.

images. Namely, G_0 and G_1 have almost the same variance and relatively strong correlation. As a result, the number of angles to be optimized and included into the bit stream is halved without degrading lossless coding performance.

This paper is organized as follows. The "non-adaptive" existing method I and the "full-adaptive" existing method II are detailed in Section II. The proposed "semi-adaptive" method with reduced computational load is described, and its simplification is endorsed in Section III. Performance of the proposed method is evaluated in respect of rounding error and compaction rate in Section IV. Conclusions are summarized in Section V.

II. EXISTING METHODS

A) Lossless coding system

In this paper, we consider the lossless coding system illustrated in Fig. 1, and discuss on a RCT for decorrelation of four color components, G_0, G_1, R, and B, acquired through Bayer pattern color filter array illustrated in Fig. 2. The reversible wavelet transform (RWT) is based on the 5/3 tap integer-type filter bank. The embedded block coding with optimal truncation points (EBCOT) is an entropy encoder [18]. Note that both of them are defined by the widely used international standard JPEG 2000 for lossless image coding [8].

B) Non-adaptive RCT (existing method I)

Figure 3 illustrates the RCT with fixed coefficients (existing method I) [9]. It converts four color components by

$$\begin{bmatrix} Y_0 \\ Y_1 \\ Y_2 \\ Y_3 \end{bmatrix} = \begin{bmatrix} G_1 - G_0 \\ F[(R + B + F[W] \cdot 2)/4] \\ R - F[W] \\ B - F[W] \end{bmatrix}, \tag{1}$$

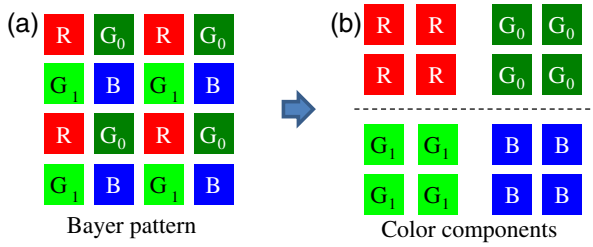

Fig. 2. Bayer pattern image and its color components.

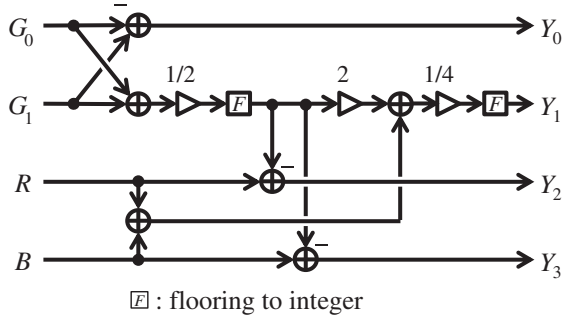

Fig. 3. Non-adaptive RCT (existing method I).

where

$$\begin{cases} W = F[(G_1 + G_0)/2], \\ F[x] = x - (x \mod 1) \end{cases}$$

and $F[x]$ denotes a floor function that converts x into integer. When the errors generated by this function is negligible, the RCT is expressed as

$$\mathbf{Y} = \mathbf{K}_4^T \cdot \mathbf{X}, \tag{2}$$

where

$$\mathbf{K}_4^T = \begin{bmatrix} -1 & 1 & 0 & 0 \\ 1/4 & 1/4 & 1/4 & 1/4 \\ -1/2 & -1/2 & 1 & 0 \\ -1/2 & -1/2 & 0 & 1 \end{bmatrix} \tag{3}$$

and

$$\begin{aligned} \mathbf{Y} &= [Y_0 \;\; Y_1 \;\; Y_2 \;\; Y_3]^T, \\ \mathbf{X} &= [G_0 \;\; G_1 \;\; R \;\; B]^T. \end{aligned} \tag{4}$$

Since the multiplier coefficients are fixed as expressed in (3), this RCT cannot be adaptive to each of input images.

C) Adaptive RCT (existing method II)

Figure 4 illustrates the RCT based on KLT (existing method II) [16]. The matrix $\mathbf{K}_4$ in (2) is determined as eigenvectors of the covariance matrix $\mathbf{R}_\mathbf{X}$ defined as

$$\mathbf{R}_\mathbf{X} = E[\mathbf{X} \cdot \mathbf{X}^T], \tag{5}$$

https://doi.org/10.1017/ATSIP.2013.6 Published online by Cambridge University Press

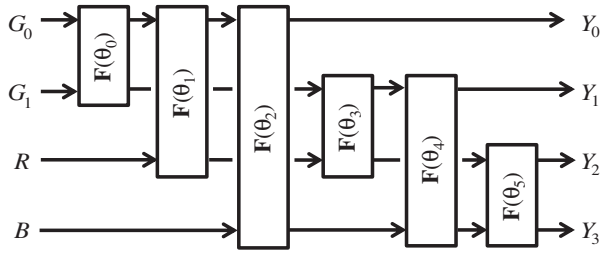

Fig. 4. Adaptive RCT (existing method II).

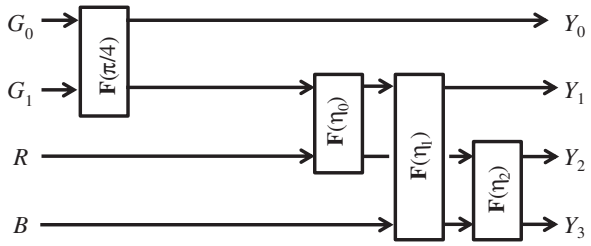

Fig. 5. Semi-adaptive RCT (proposed method).

where $E[\ ]$ denotes the ensemble average of each row and column. The KLT converts $\mathbf{R_X}$ to

$$\begin{aligned}\mathbf{R_Y} &= E[\mathbf{Y}\cdot\mathbf{Y}^T]\\ &= \mathbf{K}_4^T\cdot E[\mathbf{X}\cdot\mathbf{X}^T]\cdot\mathbf{K}_4\\ &= \mathbf{K}_4^T\cdot\mathbf{R_X}\cdot\mathbf{K}_4\\ &= diag[\lambda_0\ \ \lambda_1\ \ \lambda_2\ \ \lambda_3],\end{aligned} \tag{6}$$

where $\lambda_i, i\in\{0,1,2,3\}$ denote eigenvalues. As a result, $\mathbf{Y}$ is decorrelated adaptively to each of input color images.

The 4×4 matrix $\mathbf{K}_4$ is factorized into a product of 2×2 matrices

$$\mathbf{F}(\theta_i) = \mathbf{P}_t\cdot\mathbf{G}(\varphi_{i,t}) \tag{7}$$

for $i\in\{0,1,2,3,4,5\}$ as illustrated in Fig. 4. Each of the matrices is composed of Givens rotation

$$\mathbf{G}(\varphi_{i,t}) = \begin{bmatrix}\cos\varphi_{i,t} & -\sin\varphi_{i,t}\\ \sin\varphi_{i,t} & \cos\varphi_{i,t}\end{bmatrix} \tag{8}$$

and one of the permutations

$$\begin{aligned}\mathbf{P}_1 &= \begin{bmatrix}+1 & 0\\ 0 & +1\end{bmatrix} = \mathbf{G}(0),\\ \mathbf{P}_2 &= \begin{bmatrix}0 & +1\\ -1 & 0\end{bmatrix} = \mathbf{G}(-\pi/2),\\ \mathbf{P}_3 &= \begin{bmatrix}-1 & 0\\ 0 & -1\end{bmatrix} = \mathbf{G}(\pi),\\ \mathbf{P}_4 &= \begin{bmatrix}0 & -1\\ +1 & 0\end{bmatrix} = \mathbf{G}(+\pi/2)\end{aligned} \tag{9}$$

to avoid the singular point problem [16]. Since all the rotation angles θ_i in (7) are determined according to each of input images, this RCT is adaptive.

III. PROPOSED METHOD

A) Semi-adaptive RCT and its advantages

In this paper, we propose an RCT illustrated in Fig. 5. A redundant part of the existing method II in Fig. 4 is eliminated. The rotation angle θ_0 is fixed, and the total number of rotations $\mathbf{F}$ is reduced from six to four. In this sense, computational load is reduced. Advantages of the proposed method are summarized as below.

(i) The optimum angles to be included into the bitstream are reduced from six to three (50.0%). (ii) Size of the eigenvalue problem to be solved is reduced from 4×4 for the six angles to 3×3 for the three angles (56.3%). (iii) The total number of lifting steps, which means each equation in (10), is reduced from 18 to 12 (66.7%), since one rotation contains three lifting steps. (iv) Total delay due to the lifting steps is reduced, since a lifting step waits for a calculation result of the previous lifting step. In RCT, it accumulates and causes delay from input to output. (v) Total amount of rounding error in $Y_i, i\in\{0,1,2,3\}$ is expected to be reduced, since the rounding functions which generate the error in a lifting step are reduced. We confirm it in Section IV-A. Rational of our simplification for reduction of computational load is described in Section III-C.

B) Implementation issue

To make the transform reversible in Figs 4 and 5, the rotation $\mathbf{G}(\varphi_{i,t})$ in (7) is implemented in the lifting structure. In case of $t=1$, output signals are calculated as

$$\begin{cases}x_1' = x_1 + O[f_0\cdot x_0],\\ y_0 = x_0 + O[f_1\cdot x_1'],\\ y_1 = x_1' + O[f_2\cdot y_0],\end{cases} \tag{10}$$

with multiplier coefficients f_0, f_1, and f_2 as illustrated in "type 1" in Fig. 6. Neglecting rounding errors generated by the rounding function $O[\ ]$, Right-hand side of (7) in the lifting structure is described as

$$[y_0\ \ y_1]^T = \mathbf{P}_t\cdot\mathbf{G}(\phi_{i,t})\cdot[x_0\ \ x_1]^T, \tag{11}$$

where

$$\mathbf{G}(\varphi_{i,t}) = \begin{bmatrix}1 & 0\\ f_2 & 1\end{bmatrix}\begin{bmatrix}1 & f_1\\ 0 & 1\end{bmatrix}\begin{bmatrix}1 & 0\\ f_0 & 1\end{bmatrix} \tag{12}$$

and

$$[f_0\ \ f_1\ \ f_2] = \left[\tan\frac{\phi_{i,t}}{2},\ -\sin\phi_{i,t},\ \tan\frac{\phi_{i,t}}{2}\right]. \tag{13}$$

It indicates that the absolute value of f_0 and f_2 becomes extremely huge when the rotation angle $\varphi_{i,t}$ is close to π [rad]. It magnifies rounding error, and therefore it degrades

https://doi.org/10.1017/ATSIP.2013.6 Published online by Cambridge University Press

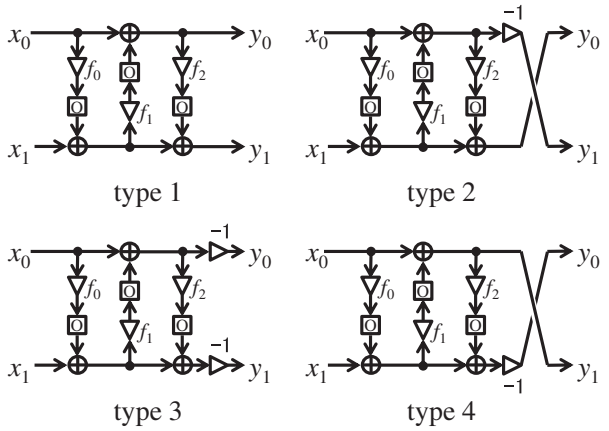

Fig. 6. Implementation of the rotation **F**.

coding efficiency. This singular point problem is avoided by selecting a proper $t \in \{1, 2, 3, 4\}$. From (7) and (9),

$$\varphi_{i,t} = \theta_i - \Theta_t \tag{14}$$

for

$$[\Theta_1\ \Theta_2\ \Theta_3\ \Theta_4] = [0\quad -\pi/2\quad \pi\quad \pi/2] \tag{15}$$

is derived. Therefore, a proper t is the one which maximizes the distance between the singular point $\varphi_{i,t} = \pi$ rad and the compensated angle $\theta_i - \Theta_t$. In this paper, we follow this procedure reported in [16].

C) Rational of the simplification

Firstly, the angle θ_0 in the existing method II is fixed to $\pi/4$ rad in our approach. This is because variance of G_0 and that of G_1 are almost the same. For example, the optimum angle θ_{opt} of a rotation $\mathbf{F}(\theta)$ is given as

$$\theta_{opt} = \frac{1}{2}\left(\frac{\pi}{2} + \arctan\frac{r-1}{2\rho}\right), \tag{16}$$

where

$$\begin{cases} r = \dfrac{\sigma_{x_1}^2}{\sigma_{x_0}^2}, \qquad \rho = \dfrac{E[(x_0 - \bar{x}_0)(x_1 - \bar{x}_1)]}{\sigma_{x_0}^2}, \\ \bar{x}_i = E[x_i], \quad \sigma_{x_i}^2 = E[(x_i - \bar{x}_i)^2], \quad i \in \{0, 1\} \end{cases} \tag{17}$$

for input signals $\mathbf{x} = [x_0\ \ x_1]$.

Equation (16) is derived as follows. Covariance matrix $\mathbf{R_X}$ of $\mathbf{X} = [x_0\ \ x_1]$ is converted to $\mathbf{R_Y}$ by the rotation $\mathbf{F}(\theta)$ as

$$\mathbf{R_Y} = \mathbf{F}^T(\theta) \cdot \mathbf{R_X} \cdot \mathbf{F}(\theta). \tag{18}$$

Substituting

$$\mathbf{F}(\theta) = \begin{bmatrix} \cos\theta & -\sin\theta \\ \sin\theta & \cos\theta \end{bmatrix}, \quad \mathbf{R_X} = \begin{bmatrix} 1 & \rho \\ \rho & r \end{bmatrix}\sigma_{x_0}^2, \tag{19}$$

we have

$$\frac{\mathbf{R_Y}}{\sigma_{x_0}^2} = \mathbf{I}_2 + \begin{bmatrix} 1-c & s \\ s & 1+c \end{bmatrix} \cdot \frac{r-1}{2} + \begin{bmatrix} s & c \\ c & -s \end{bmatrix} \cdot \rho \tag{20}$$

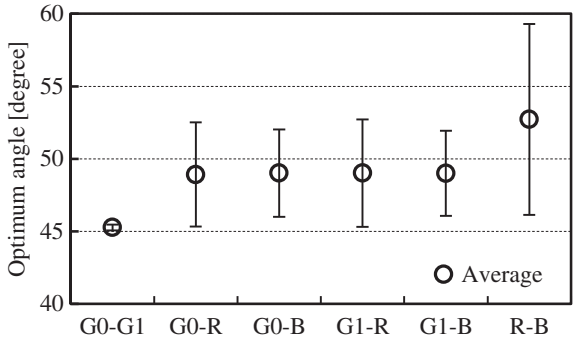

Fig. 7. Optimum angle of the rotation $\mathbf{F}(\theta)$ for images.

for $[c\ \ s] = [\cos 2\theta\ \ \sin 2\theta]$ and $\mathbf{I}_2 = diag[1\ 1]$. Therefore, when it becomes uncorrelated,

$$s \cdot \frac{r-1}{2} + c \cdot \rho = 0 \tag{21}$$

holds. Since it is equivalent to

$$\sqrt{\left(\frac{r-1}{2}\right)^2 + \rho^2} \cdot \cos\left(2\theta - \operatorname{atctan}\frac{r-1}{2\rho}\right) = 0, \tag{22}$$

we have the equation equivalent to (16) as

$$2\theta_{opt} - \operatorname{atctan}\frac{r-1}{2\rho} = \frac{\pi}{2}. \tag{23}$$

According to (16) and (17), $\theta_{opt} = \pi/4$ [rad] for $r = 1$ in which variance of x_0 and that of x_1 is the same. This is experimentally endorsed for several images as summarized in Fig. 7. Note that the tested images are subsampled to generate Bayer-type four color components and used for evaluation. The angle varies depending on input images. Standard deviation was observed to be 6.58° for $[x_0\ \ x_1] = [R\quad B]$ at maximum. It is 0.20° for $[x_0\ \ x_1] = [G_0\ \ G_1]$, namely the angle can be fixed.

Secondly, both of the angles θ_1 and θ_2 in the existing method II are set to zero. This is because variance of Y_0 in Fig. 5 is close to zero. It comes from a fact that correlation between G_0 and G_1 is close to one. For example, variance of

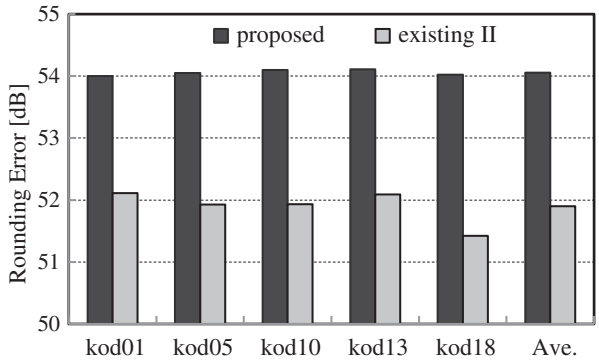

Fig. 8. Evaluation of rounding error.

https://doi.org/10.1017/ATSIP.2013.6 Published online by Cambridge University Press

Table 1. The average code length of images in [bpp] for KODAK image set.

	Tint −100			Tint 0			Tint +100		
	Existing			Existing			Existing		
Image	I	II	Proposed	I	II	Proposed	I	II	Proposed
kod01	6.14	**6.07**	6.09	5.99	**5.95**	5.99	5.91	5.75	**5.74**
kod05	6.51	**6.44**	**6.44**	6.35	**6.32**	6.33	6.36	6.23	**6.21**
kod10	4.48	4.46	**4.44**	4.38	**4.34**	4.35	4.36	4.31	**4.26**
kod13	**6.65**	6.67	6.70	6.59	**6.54**	6.58	6.61	6.59	**6.56**
kod18	5.96	5.93	**5.92**	5.85	5.85	**5.83**	5.84	**5.72**	**5.72**
Ave.	5.95	**5.91**	5.92	5.83	**5.80**	5.81	5.82	5.72	**5.70**

Table 2. The average code length of images in [bpp] for SIDBA image set.

	Tint −100			Tint 0			Tint +100		
	Existing			Existing			Existing		
Image	I	II	Proposed	I	II	Proposed	I	II	Proposed
Airplane	4.86	**4.80**	4.77	4.79	4.77	**4.76**	4.84	4.68	**4.64**
Lenna	**5.23**	5.27	5.26	**5.13**	5.14	**5.13**	5.13	**5.01**	**5.01**
Milkdrop	4.71	4.68	**4.66**	4.59	4.52	**4.50**	4.60	**4.43**	**4.43**
Pepper	5.39	5.38	**5.37**	5.35	5.30	**5.29**	5.41	5.16	**5.14**
Sailboat	5.89	**5.86**	5.87	5.89	5.85	**5.85**	6.01	5.88	**5.86**
Ave.	5.21	5.20	**5.19**	5.15	**5.11**	**5.11**	5.20	5.03	**5.02**

Y_0 is given as

$$\sigma_{Y_0}^2 = \frac{\sigma_{x_0}^2}{2}(1 + r - 2\rho) \tag{24}$$

for $\mathbf{x} = [x_0 \;\; x_1]$. This equation is derived as follows. Since Y_0 is the first row of the matrix

$$\mathbf{Y} = \mathbf{F}^T(\pi/4) \cdot \mathbf{X}, \tag{25}$$

its variance is given as

$$\sigma_{Y_0}^2 = E\left[\left(\frac{x_0 - x_1}{\sqrt{2}}\right)^2\right] = \frac{E[x_0^2] + E[x_1^2] - 2E[x_0 x_1]}{2}, \tag{26}$$

which is equivalent to (24).

As described above, it becomes almost zero for $r = 1$ and $\rho = 1$. It is no use to rotate this component with other component. Therefore, rotations $\mathbf{F}(\theta_1)$ and $\mathbf{F}(\theta_2)$ can be eliminated. Namely, we simplified the existing method II utilizing a fact that statistical relation between the two green components G_0 and G_1 is fixed for various input images. The procedure itself is very simple. In the next section, we experimentally investigate its coding performance based on (1) rounding error, (2) adaptability, and (3) compaction rate.

IV. EXPERIMENTAL RESULTS

A) Rounding error

Figure 8 illustrates evaluation results of rounding errors included in Y_0, Y_1, Y_2, and Y_3. The error is defined as difference between output of an RCT with rounding function and that of the same RCT without rounding. Total amount of variance of the error is measured in peak signal to noise ratio (PSNR) defined as

$$PSNR = 10\log_{10} 255^2 - 10\log_{10} \sum_{i=0}^{3} \sigma_i^2 \quad [\text{dB}], \tag{27}$$

where σ_i denotes the standard deviation of the error in Y_i. PSNR of the proposed method was observed to be 54.1 dB in average for images. It is greater than the existing method II by 2.2 dB. Reduction of the rounding functions is considered to contribute to this improvement.

B) Adaptability and compaction rate

Table 1 summarizes evaluation results of data compaction rate for KODAK test images. Since this data set was reported to have considerably high correlations [19], we also used SIDBA data set and RAW images taken with Nikon D80 camera. For these images, results are summarized in Tables 2 and 3, respectively.

The compaction rate was measured with the average code length defined as the ratio of total amount of compressed binary data and the total number of pixels in the image. Note that it indicates 8 bit per pixel per component [bpp], when the data volume is not compressed at all. "Tint" indicates parameter of color balancing in Paint Shop Pro X3. Figures 9–11 illustrate examples of sample images at different value of "Tint".

Table 4 indicates the average code length for all the images in Tables 1–3. In case of "Tint 0", the existing

https://doi.org/10.1017/ATSIP.2013.6 Published online by Cambridge University Press

Table 3. The average code length of images in [bpp] for RAW images taken with Nikon D80 camera.

	Tint −100			Tint 0			Tint +100		
	Existing			Existing			Existing		
Image	I	II	Proposed	I	II	Proposed	I	II	Proposed
Car	**3.58**	3.63	3.60	3.65	3.57	**3.51**	3.97	3.65	**3.56**
Castle	3.81	**3.79**	3.86	3.94	**3.90**	3.93	4.01	3.78	**3.76**
Close up	5.02	5.01	**5.00**	4.96	**4.94**	**4.94**	5.12	**5.00**	**5.00**
Portrait	5.22	**5.21**	5.22	5.13	**5.12**	**5.12**	5.12	**5.02**	5.03
Scenery	3.66	**3.63**	3.64	3.74	3.53	**3.52**	4.00	3.42	**3.37**
Ave.	4.26	**4.25**	4.26	4.28	4.21	**4.20**	4.44	4.17	**4.14**

Fig. 9. Sample image "Kodo5" at different value of "Tint".

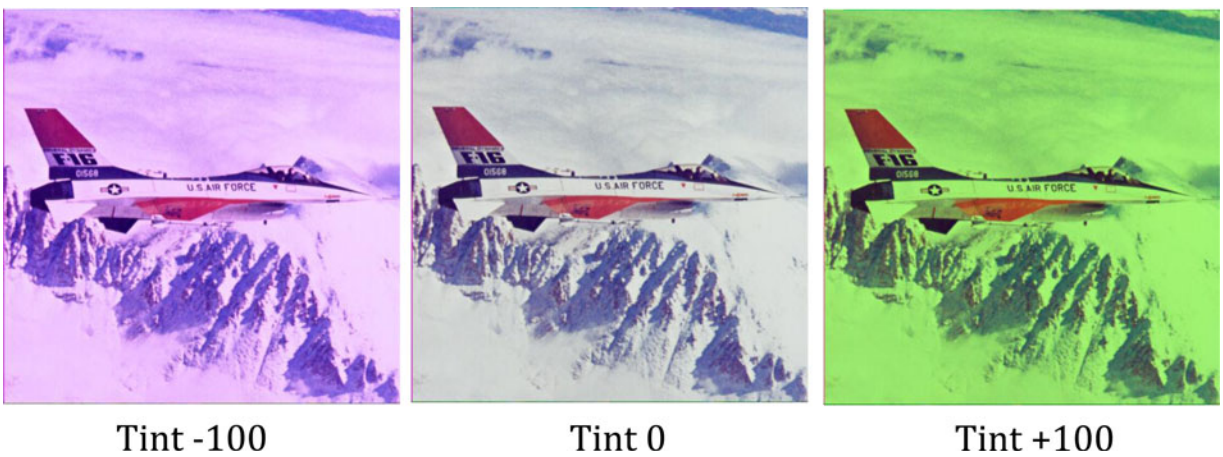

Fig. 10. Sample image "Airplane" at different "Tint".

https://doi.org/10.1017/ATSIP.2013.6 Published online by Cambridge University Press

Fig. 11. Sample image "Scenery" at different "Tint".

Table 4. The average code length of all the images in [bpp].

	Tint-100			Tint 0			Tint + 100		
	Existing			Existing			Existing		
Average of all images	I	II	Proposed	I	II	Proposed	I	II	Proposed
	5.14	**5.12**	**5.12**	5.09	**5.04**	**5.04**	5.15	**4.98**	**4.95**

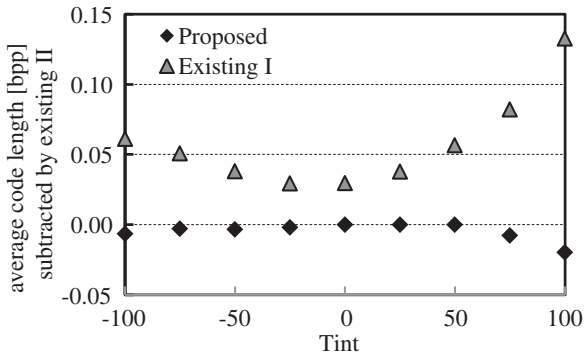

Fig. 12. The average code length subtracted by the existing method II for a sample image "Kodo5".

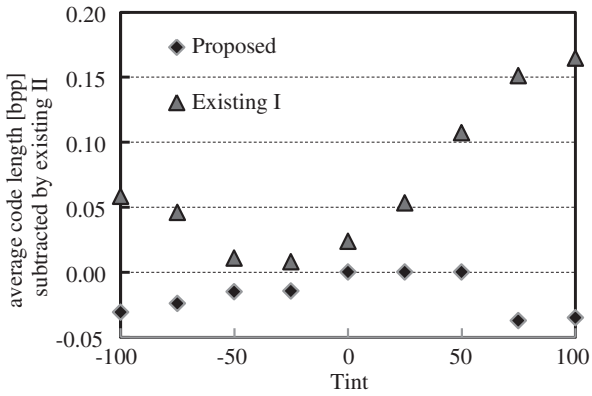

Fig. 13. The average code length subtracted by the existing method II for a sample image "airplane".

method II and the proposed method are the same. Those are superior to the existing method I by 0.05 bpp. However, there is no significant difference. On the contrary, in case of "Tint +100", the proposed method is the best, and the existing method I is the worst. The difference was observed to be 0.20 bpp in average.

Figures 12–14 illustrate the average code length of the existing method I and the proposed method for a sample image in Figs 9–11, respectively. These are subtracted by that of the existing method II. There is no significant difference between the existing method II and the proposed method. It means that the proposed method keeps adaptability of the existing method II, even though signal processing is simplified. It also indicates that the existing method I is not adaptive. This is because its multiplier coefficients are fixed as indicated in (3).

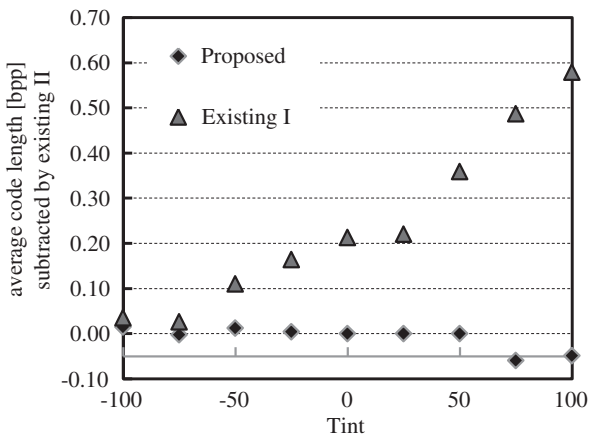

Fig. 14. The average code length subtracted by the existing method II for a sample image "scenery".

https://doi.org/10.1017/ATSIP.2013.6 Published online by Cambridge University Press

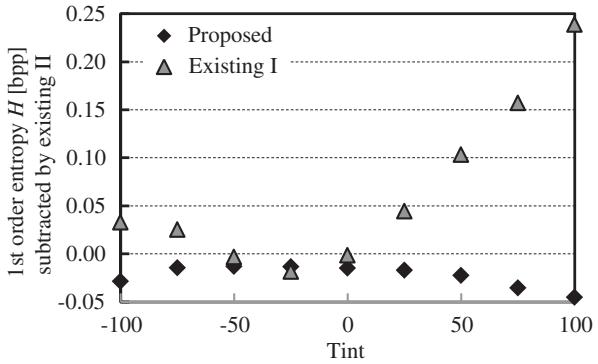

Fig. 15. The first-order entropy H subtracted by that of the existing method II for "for a sample image "Kodo5".

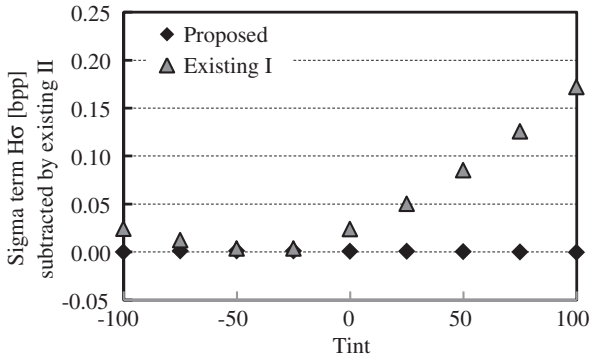

Fig. 16. The sigma term H_σ in the first-order entropy H. It is subtracted by that of the existing method II.

C) Discussions on improvement of compaction rate

As a result of our experiments, it was observed that the proposed method attains almost the same coding performance as the existing method II, even though its computational load is reduced. Remarkably, the proposed method is slightly better than the existing method II for *greenish* images with "Tint +100". In the rest of this paper, we endorse it with theoretical analysis on entropy rate and probability density function (PDF) of signals inside the RCT.

Figure 15 illustrates the first-order entropy H, which is defined as

$$H = \frac{1}{4}\sum_{i=0}^{3}\sum_{j} W_j \cdot H_{i,j}, \tag{28}$$

where

$$H_{i,j} = -\sum_{x_{i,j}} P(x_{i,j}) \log_2 P(x_{i,j}) \tag{29}$$

and $x_{i,j}$ denotes the pixel value in jth frequency band of the RWT in ith component. W_j denotes the ratio of the total number of pixels in jth band to all the number of pixels in each component. The entropy H is determined by the PDF of $x_{i,j}$, and it estimates the average code length illustrated in Fig. 12.

Figures 16 and 17 illustrate the sigma term H_σ and the epsilon term H_ε of the first-order entropy H, respectively. Those are defined as

$$H = H_\sigma + H_\varepsilon \tag{30}$$

where

$$\begin{cases} H_\sigma = -\dfrac{1}{2}\log_2 \displaystyle\prod_{i=0}^{3}\prod_{j}(\sigma_{i,j}^2)^{W_j/4} \\ H_\varepsilon = -\dfrac{1}{2}\log_2 \displaystyle\prod_{i=0}^{3}\prod_{j}(\varepsilon_{i,j}^2)^{W_j/4} \end{cases} \tag{31}$$

for standard deviation $\sigma_{i,j}$ of $x_{i,j}$. A parameter $\varepsilon_{i,j}$ is determined by shape of the PDF [20]. Figure 16 indicates that

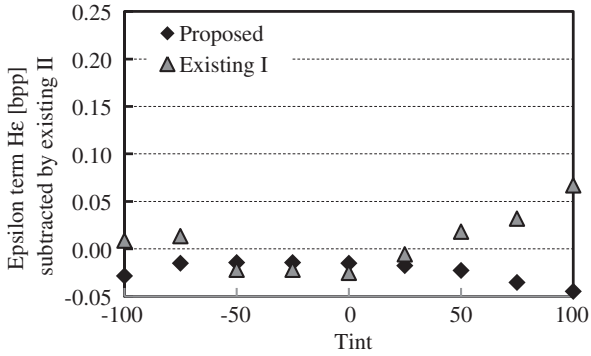

Fig. 17. The epsilon term H_ε in the first-order entropy H, which is subtracted by that of the existing method II. (a) Existing method II (KLD = 0.09) (b) Proposed method (KLD = 0.33).

there is no difference between the existing method II and the proposed method in respect of the coding gain, which is often used for theoretical evaluation of lossless coding assuming that shape of all the PDF are the same. On the contrary, Fig. 17 indicates superiority of the proposed method to the existing method II. As a result, it was found that superiority of the proposed method comes from suitability of shape of PDF.

Finally, we compare the existing method II and the proposed method in respect of shape of PDF. In Fig. 18(a), "Existing II" indicates histogram of signal values of Y_0 in Fig. 4, and "Gaussian" indicates the Gaussian function:

$$G(x) = \frac{1}{\sqrt{2\pi}\sigma}\exp\left\{-\left(\frac{(x-\mu)^2}{2\sigma^2}\right)\right\} \tag{32}$$

with zero mean $\mu = 0$ and the same variance σ as the signal values of Y_0. Similarly, "Proposed" in Fig. 18(b) indicates histogram of signal values of Y_0 in Fig. 5. Comparing these figures, it is observed that "existing II" is closer to "Gaussian" than "Proposed". This is numerically endorsed with the Kullback–Leibler divergence defined by

$$KLD(P\|Q) = \sum_{k} P(k)\log\frac{P(k)}{Q(k)}, \tag{33}$$

https://doi.org/10.1017/ATSIP.2013.6 Published online by Cambridge University Press

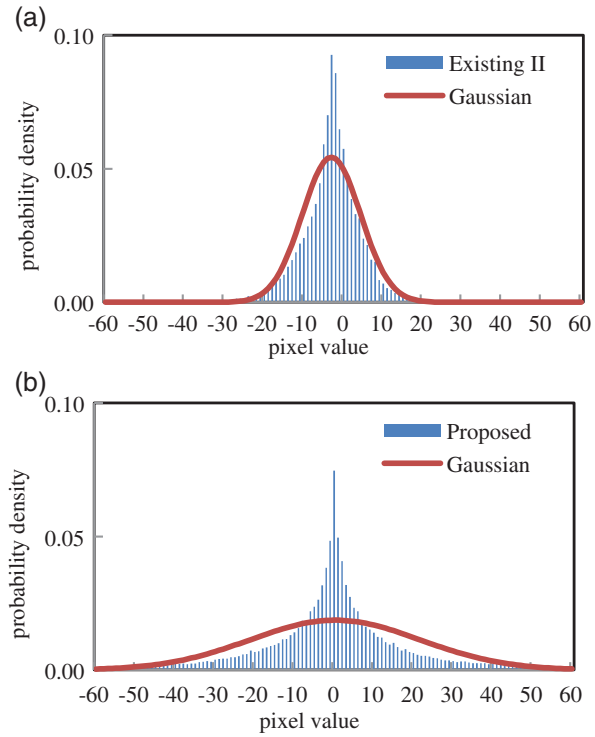

Fig. 18. PDF and KLD.

where k denotes the pixel value. In this case, $Q(k)$ is set to Gaussian function with the same variance as that of Y_0. It is observed that KLD of the existing method II is 0.09, which is smaller than that of the proposed method by 0.24.

It can be considered that PDF tends to become Gaussian-like shape according to the central limit theorem in the existing method II, due to more lifting steps than the proposed method. In conclusion, it was indicated that simplification of the proposal in this paper (reduction of the number of lifting steps) keeps "good" shape of PDF, and contributes to improving coding performance. However, there is some room for further investigation.

V. CONCLUSIONS

In this paper, we simplified an existing KLT-based RCT, maintaining its adaptability to various Bayer color filter array images. We removed a redundant part of its lifting steps, utilizing a fact that G_0 and G_1 have almost the same variance and relatively strong correlation.

As a result, overhead to be included into the bit-stream, size of the eigenvalue problem and the total number of lifting steps are reduced to 50.0, 56.3, and 66.7%, respectively. Total amount of rounding error is confirmed to be reduced by 2.2 dB. Even though its computational load is reduced, it was observed that the proposed method attains slightly better coding performance. We endorsed it with theoretical analysis on the entropy and PDF of signals inside the RCT. However, further investigation is necessary in the future.

ACKNOWLEDGEMENTS

This work was supported by KAKENHI (grant no. 23560445).

REFERENCES

[1] Matsuda, I.; Kaneko, T.; Minezawa, A. Itoh, S.: Lossless coding of color images using block-adaptive inter-color prediction. In *IEEE Int. Conf. on Image Processing (ICIP)*, no.II, 2007, 329–332.

[2] Kaneko, T.; Matsuda, I.; Itoh, S.: Lossless coding of bayer color filter array images using block-adaptive prediction. J. Inst. Image Inf. Telev. Eng., **62**(11) (2008), 1840–1843.

[3] Chung, K.H.; Chan, Y.H.: A lossless compression scheme for Bayer color filter array images. IEEE Trans. Image Process., **17**(2) (2008), 134–143.

[4] Zhang, N.; Wu, X.: Lossless compression of color mosaic images. IEEE Trans. Image Process., **15**(6) (2006), 1379–1388.

[5] Bayer, B.E.: Color Imaging Array, *Eastman Kodak Company*, Rochester, NY, U.S. 3971065, 1976.

[6] ISO/IEC JTC 1/SC 29/WG 1 N1687. 'JPEG-LS part-2' (14495–2). FCD Ver. 1.0, April 2000.

[7] Wu, X.; Memon, N.: Context-based, adaptive, lossless image coding. IEEE Trans. Commun., **45**(5) (1997), 437–444.

[8] ISO/IEC FCD15444-1: JPEG 2000 image coding system. March 2000.

[9] Olympus corp. Patent No.4436733, Japan, March 2006.

[10] Malvar, H.S.; Sullivan, G.J.; Srinivasan, S.: Lifting-based reversible color transformations for image compression. SPIE, 7073, pp. 1–10. 2008.

[11] Van Assche, S.; Philips, W.; Lemahieu, I.: Lossless compression of pre-press images using a novel color decorrelation technique. Pattern Recognit., **32** (1999), 435–441.

[12] Dragotti, P.L.; Poggi, G.; Ragozini, A.R.P.: Compression of multispectral images by three-dimensional SPIHT algorithm. IEEE Trans. Geosci. Remote Sens., **38**(1) (2000), 416–428.

[13] Soo-Chang, P.; Jian-Jiun, D.: Reversible integer color transform. IEEE Trans. Image Process., **16**(6) (2007), 1686–1691.

[14] Benazza-Benyahia, A.; Pesquet, J.C.; Hamdi, M.: Vector-lifting schemes for lossless coding and progressive archival of multispectral images. IEEE Trans. Geosci. Remote Sens., **40**(9) (2002), 2011–2024.

[15] Hao, P.; Shi, Q.: Reversible Integer KLT for progressive-to-lossless compression of multiple component images. In *IEEE Int. Conf. Image Processing (ICIP)*, vol. 1, 2003, 633–636.

[16] Iwahashi, M.; Kiya, H.: Optimization of lifting structure of reversible KLT based on permutation of signal's order and sign. In *IEEE Int. Conf. Image Processing (ICIP)*, no. MA-PD.7, 2010, 465–468.

[17] Iwahashi, M.; Ogawa, M.; Kiya, H.: Avoidance of singular point in integer orthonormal transform for lossless coding. IEEE Trans. Signal Process., **60**(5) (2012), 2648–2653.

[18] Taubman, D.: High performance scalable image compression with EBCOT. IEEE Trans. Image Process., **9**(7) (2000), 1158–1170.

[19] Zhang, F.; Wu, X.; Yang, X.; Zhang, W.; Zhang, L.: Robust color demosaicking with adaptation to varying spectral correlations. IEEE Trans. Image Process., **18**(12) (2009), 2706–2717.

[20] Jayant, N.S.; Noll, P.: Digital Coding of Waveforms. *Prentice-Hall*, New Jersey, Table 4.8, 1984, 154.

https://doi.org/10.1017/ATSIP.2013.6 Published online by Cambridge University Press

Suvit Poomrittigul received the B.E. degree in Telecommunication Engineering from King Mongkut's Institute of Techntology Ladkrabang, Thai11and in 2005 and M.E. degrees in Computer Engineering from Chulalongkorn University, Thailand in 2009, respectively. He is currently a doctoral student of Information Science and Control Engineering Department in Nagaoka University of Technology.

Masanori Ogawa received the B.E. and M.E. degrees in Electrical Engineering from Nagaoka University of Technology in 2010 and 2012, respectively. His research interests are in the area of digital signal processing, multi-rate systems, and image compression.

Masahiro Iwahashi received his B.E., M.E., and D.E. degrees in electrical engineering from Tokyo Metropolitan University in 1988, 1990, and 1996, respectively. In 1990, he joined Nippon Steel Co. Ltd. From 1991 to 1992, he was dispatched to Graphics Communication Technology Co. Ltd. In 1993, he joined Nagaoka University of Technology, where he is currently a professor of Department of Electrical Engineering, Faculty of Technology. From 1995 to 2001, he served concurrently as a lecturer of Nagaoka Technical College. From 1998 to 2001, he was dispatched to Thammasat University, Thailand, and to the Electronic Engineering Polytechnic Institute of Surabaya, Indonesia, as a JICA expert. His research interests are in the area of digital signal processing, multi-rate systems, and image compression. He served as an editorial committee member of the transaction on fundamentals of IEICE from 2007 to 2011. He is currently serving as a technical committee member of Image Engineering, and a permanent reviewer of IEICE. He is also serving as a reviewer of ICASSP, ICIP and transaction on IP, SP, and CASVT of the IEEE. He is currently a member of APSIPA, and a senior member of IEEE.

Hitoshi Kiya received his B.E. and M.E. degrees from Nagaoka University of Technology, Japan, in 1980 and 1982, respectively, and his Dr. Eng. degree from Tokyo Metropolitan University in 1987. In 1982, he joined Tokyo Metropolitan University as an Assistant Professor, where he became a Full Professor in 2000. From 1995 to 1996, he attended the University of Sydney, Australia as a Visiting Fellow. He currently serves as a Vice President of APSIPA, a Member of the Board of Governor of APSIPA, the Vice Chair of IEEE SPS Japan Chapter, an Associate Editor of IEEE Trans. Image Processing and of ISRN Signal Processing, and the Publications Board Chair of IEICE ES Society, respectively. He also served as the President of IEICE ES Society, an Associate Editor of IEEE Trans. Signal Processing, the Editor-in-Chief of IEICE Fundamentals Review. His research interests are in the area of signal and image processing including multirate signal processing, wavelets, video coding, compressed-domain video manipulation, and security for multimedia. He received the ITE Niwa Takayanagi Best Paper Award in 2012, the Telecommunications Advancement Foundation Award in 2011, the IEICE ESS Contribution Award in 2010, and the IEICE Best Paper Award in 2008. He is a Fellow Member of the ITE, IEICE and a Senior Member of the IEEE.

https://doi.org/10.1017/ATSIP.2013.6 Published online by Cambridge University Press